calculating the losses due to a finite κ. In mathematical notation, this reads

$$\lim_{t\to 0}\left[\lim_{\kappa\to\infty}\Big|_{\delta(\kappa)\ll t}\cdots\right]\neq\lim_{\kappa\to\infty}\left[\lim_{t\to 0}\cdots\right].$$

III. Conclusions

When calculating the conductor loss of planar transmission lines by means of perturbation methods, the assumption of zero strip thickness becomes critical: the surface current integral at the strip edges does not exist. In the numerical analysis, the results for the attenuation constant do not converge. For an increasing number M of spectral eigenfunctions, α_c approaches infinity. However, α_c shows a logarithmic dependence on M so that, in practice, the unbounded behavior may be easily overlooked or misinterpreted. As a consequence, attenuation results obtained on the basis of zero-strip-thickness approaches, such as the common spectral-domain technique, should be handled very critically and checked against measurements.

Acknowledgment

The authors are grateful to Prof. H. L. Hartnagel for his continuous support and encouragement.

References

[1] D. Mirshekar-Syahkal and J. B. Davies, "Accurate solution of microstrip and coplanar structures for dispersion and for dielectric and conductor losses," *IEEE Trans. Microwave Theory Tech.*, vol. MTT-27, pp. 694–699, July 1979.

[2] D. Mirshekar-Syahkal and J. B. Davies, "An accurate, unified solution to various fin-line structures, of phase constant, characteristic impedance, and attenuation," *IEEE Trans. Microwave Theory Tech.*, vol. MTT-30, pp. 1854–1861, Nov. 1982.

[3] H. J. Finlay, R. H. Jansen, J. A. Jenkins, and I. G. Eddison, "Accurate characterization and modeling of transmission lines for GaAs MMIC's," *IEEE Trans. Microwave Theory Tech.*, vol. 36, pp. 961–967, June 1988.

[4] R. Pregla, "Determination of conductor losses in planar waveguide structures," *IEEE Trans. Microwave Theory Tech.*, vol. MTT-28, pp. 433–434, Apr. 1980.

[5] P. Heitkämper, "Berechnung von planaren Leiterstrukturen mit Hilfe der Spektralbereichsmethode" (in German), Studienarbeit St 1528, Technische Hochschule Darmstadt, 1990 (unpublished).

A Closed-Form Spatial Green's Function for the Thick Microstrip Substrate

Y. L. Chow, J. J. Yang, D. G. Fang, and G. E. Howard

Abstract—**The spatial Green's function for the open microstrip structure, especially with a thick substrate, is generally represented by time-consuming Sommerfeld integrals. In this paper, through the Sommerfeld identity, a closed-form spatial Green's function of a few terms is found from the quasi-dynamic images, the complex images, and the surface waves. With the numerical integration of the Sommerfeld integrals thus avoided, this closed-form Green's function is computationally very efficient. Numerical examples show that the closed-form Green's function gives less than 1% error for all substrates and source-to-field distances.**

Manuscript received May 15, 1990; revised October 22, 1990. This work was supported by the Communications Research Center, Canada, under Contract 36001-9-3581/01-SS, and by the Natural Science Foundation of the People's Republic of China.

Y. L. Chow, J. J. Yang, and G. E. Howard are with the Department of Electrical and Computer Engineering, University of Waterloo, Waterloo, Ont., Canada N2L 3G1.

D. G. Fang is with the East China Institute of Technology, Nanjing, China 210014.

IEEE Log Number 9041951.

I. Introduction

In the modeling of microwave integrated circuits (MIC's) and microstrip antennas, much effort has to be dedicated to the computation of Sommerfeld integrals. For a thin microstrip substrate, say $h/\lambda_\epsilon < 0.05$, the quasi-dynamic image model intuitively developed by Chow [1] is a good replacement for the Sommerfeld integrals. For a thick substrate and when the distance from the source point to the field point is great, however, this replacement deteriorates because of its neglect of the surface and leaky wave effects. To accurately model the thick-substrate microstrip circuits, it appears that the time-consuming numerical integration of Sommerfeld integrals has to be performed [2], [3]. Although the exact image method was developed for the microstrip structure [4], where the Sommerfeld integrals were replaced by certain alternative infinite integrals, it was shown in [5] that this alternative type of numerical integration is still rather time-consuming.

In this paper, a closed-form Green's function for a thick microstrip substrate is presented. This Green's function consists of three parts: $G = A + B + C$, where A represents the contribution from a few *quasi-dynamic images* dominating in the near-field region, C represents the contribution from *surface waves* dominating in the far-field region of the substrate surface, and B represents the contribution from the *complex images*, which are related to leaky waves and are very important in the intermediate field region. With this closed form, numerical integration of Sommerfeld integrals is completely avoided. It will be shown below numerically that at any frequency, this closed-form Green's function gives less than 1% error compared with the numerical integration of Sommerfeld integrals in the whole range of substrate surfaces.

II. Theory

Consider an x-directed electric dipole of unit strength located above a microstrip substrate, as shown in Fig. 1. The spectral-domain potentials in the air region can be represented as follows:

$$\tilde{G}_A^{xx} = \frac{\mu_0}{4\pi}\frac{1}{j2k_{z0}}\left[e^{-jk_{z0}(z-z')} + R_{\mathrm{TE}}e^{-jk_{z0}(z+z')}\right] \tag{1a}$$

$$\tilde{G}_q = \frac{1}{4\pi\epsilon_0}\frac{1}{j2k_{z0}}\left[e^{-jk_{z0}(z-z')} + \left(R_{\mathrm{TE}}+R_q\right)e^{-jk_{z0}(z+z')}\right] \tag{1b}$$

where

$$R_{\mathrm{TE}} = -\frac{r_{10}^{\mathrm{TE}} + e^{-j2k_{z1}h}}{1 + r_{10}^{\mathrm{TE}}e^{-j2k_{z1}h}} \tag{2a}$$

$$R_q = \frac{2k_{z0}^2(1-\epsilon_r)(1-e^{-j4k_{z1}h})}{(k_{z1}+k_{z0})(k_{z1}+\epsilon_r k_{z0})\left(1+r_{10}^{\mathrm{TE}}e^{-j2k_{z1}h}\right)\left(1-r_{10}^{\mathrm{TM}}e^{-j2k_{z1}h}\right)} \tag{2b}$$

$$r_{10}^{\mathrm{TE}} = \frac{k_{z1}-k_{z0}}{k_{z1}+k_{z0}} \qquad r_{10}^{\mathrm{TM}} = \frac{k_{z1}-\epsilon_r k_{z0}}{k_{z1}+\epsilon_r k_{z0}} \tag{3}$$

$$k_{z0}^2 + k_\rho^2 = k_0^2 \qquad k_{z1}^2 + k_\rho^2 = \epsilon_r k_0^2. \tag{4}$$

In (1), $\tilde{G}_A^{xx}$ stands for the x component of spectral-domain vector potential $\vec{A}$ created by the x-directed electric dipole, and $\tilde{G}_q$ stands for the spectral-domain scalar potential associated with one charge of the dipole. R_{TE} and R_q take into account the effects of the microstrip substrate. The spectral-domain Green's functions of (1) were given in a more compact form by

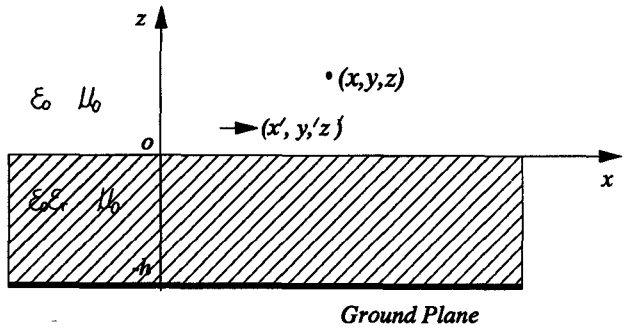

Fig. 1. The open microstrip structure.

Mosig and Gardiol [2]. Here we write them in the form of plane wave summations. It can be seen below that this form is physically clearer for deriving the quasi-dynamic and complex images.

A. Sommerfeld Integrals with a Deformed Integration Path

Making the inverse Hankel transformation to the spectral-domain Green's function in (1), and using the Sommerfeld identity [6] on the first exponential term, we can get the following spatial-domain Green's functions in Sommerfeld integral form:

$$G_A^{xx} = \frac{\mu_0}{4\pi}\left(\frac{e^{-jk_0 r_0}}{r_0} + \int_{-\infty}^{+\infty} \frac{1}{j2k_{z0}} R_{\mathrm{TE}} e^{-jk_{z0}(z+z')} \cdot H_0^{(2)}(k_\rho \rho) k_\rho \, dk_\rho\right) \tag{5a}$$

$$G_q = \frac{1}{4\pi\epsilon_0}\left(\frac{e^{-jk_0 r_0}}{r_0} + \int_{-\infty}^{+\infty} \frac{1}{j2k_{z0}} (R_{\mathrm{TE}} + R_q) e^{-jk_{z0}(z+z')} \cdot H_0^{(2)}(k_\rho \rho) k_\rho \, dk_\rho\right) \tag{5b}$$

where

$$r_0 = \sqrt{\rho^2 + (z-z')^2}.$$

The integration can be performed along the real axis C_0 on the complex k_ρ plane or along any other deformed path C_1 passing through the origin and lying in the first and third quadrants, as shown in Fig. 2(a). The integration path C_0 can be deformed to C_1, since no singularity is encountered in the deformation. The corresponding paths of C_0 and C_1 on the complex k_{z0} plane are shown in Fig. 2(b). The deformed path C_1 is of special importance in finding the complex images and will be discussed in subsection II-D.

B. Extraction of Quasi-Dynamic Images

It is seen from (4) that if the frequency is equal to zero, then $k_0 = 0$ and $k_{z0} = k_{z1}$. Therefore when the frequency is low, we can use the approximation $k_{z0} \approx k_{z1}$, and R_{TE} and R_q can thus be reduced to the quasi-dynamic forms:

$$R_{\mathrm{TE}} \to R_{\mathrm{TE0}} = -e^{-j2k_{z0}h} \tag{6a}$$

$$R_q \to R_{q0} = \frac{K(1-e^{-j4k_{z0}h})}{1-Ke^{-j2k_{z0}h}} \tag{6b}$$

where $K = (1-\epsilon_r)/(1+\epsilon_r)$. Extracting the above quasi-dynamic terms from the integrands in (5) and using the Sommerfeld

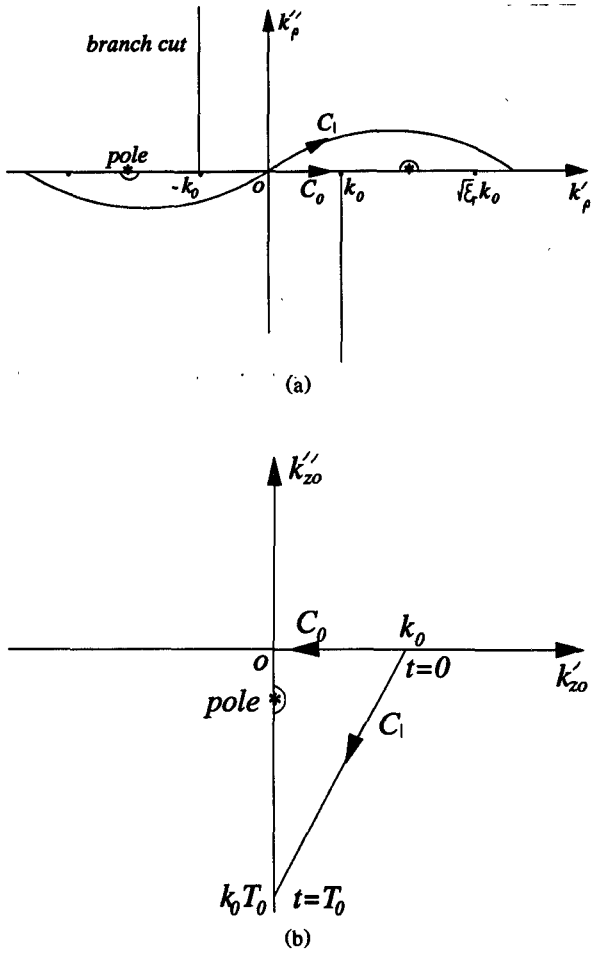

Fig. 2. (a) The integration contours C_0 and C_1 on the complex k_ρ plane. (b) The integration contours C_0 and C_1 on the complex k_{z0} plane.

identity, we can rewrite (5) as follows:

$$G_A^{xx} = G_{A0}^{xx} + \frac{\mu_0}{4\pi}\int_{-\infty}^{+\infty} \frac{1}{j2k_{z0}} (R_{\mathrm{TE}} - R_{\mathrm{TE0}}) \cdot e^{-jk_{z0}(z+z')} H_0^{(2)}(k_\rho \rho) k_\rho \, dk_\rho \tag{7a}$$

$$G_q = G_{q0} + \frac{1}{4\pi\epsilon_0}\int_{-\infty}^{+\infty} \frac{1}{j2k_{z0}} (R_{\mathrm{TE}} + R_q - R_{\mathrm{TE0}} - R_{q0}) \cdot e^{-jk_{z0}(z+z')} H_0^{(2)}(k_\rho \rho) k_\rho \, dk_\rho \tag{7b}$$

where

$$G_{A0}^{xx} = \frac{\mu_0}{4\pi}\left(\frac{e^{-jk_0 r_0}}{r_0} - \frac{e^{-jk_0 r'_0}}{r'_0}\right) \tag{8a}$$

$$G_{q0} = \frac{1}{4\pi\epsilon_0}\left(\frac{e^{-jk_0 r_0}}{r_0} + K\frac{e^{-jk_0 r''_0}}{r''_0} + \sum_{n=1}^{\infty} K^{n-1}(K^2-1)\frac{e^{-jk_0 r_n}}{r_n}\right) \tag{8b}$$

$$r'_0 = \sqrt{\rho^2 + (z+z'+2h)^2} \qquad r''_0 = \sqrt{\rho^2 + (z+z')^2}$$

$$r_n = \sqrt{\rho^2 + (z+z'+2nh)^2}.$$

Expression (8) stands for the quasi-dynamic image model intuitively developed by Chow [1]. It is pointed out in [1] that the Faraday field (related to $\vec{A}$) is not affected by the dielectric interfaces, while the Coloumb field is affected by the dielectric

interfaces through an infinite number of images. From the viewpoint of spectral-domain analysis, this quasi-dynamic model is a low-frequency approximation of the full-wave solution.

It has been pointed out by Dai and Chow [7] that when ϵ_r is large, G_{q0} in (8b) is a slowly convergent series. For instance, if $\epsilon_r = 12.9$, $h/\lambda_0 = 0.05$, as many as 80 terms should be taken to ensure the convergence. In [7], a reduced image model was presented, in which only four images are necessary. Such reduction is not necessarily unique. Here a simpler alternative reduced image scheme is given below.

Expanding the R_{q0} of (6b) in Taylor series and taking only the two leading terms, we have

$$R_{q0} \approx K(1 - e^{-j4k_{z0}h})(1 + Ke^{-j2k_{z0}h}). \tag{9}$$

Corresponding to (9), the quasi-dynamic Green's function for the scalar potential should be as follows:

$$G_{q0} = \frac{1}{4\pi\epsilon_0}\left(\frac{e^{-jk_0r_0}}{r_0} + K\frac{e^{-jk_0r_0''}}{r_0''} + K^2\frac{e^{-jk_0r_1}}{r_1} - \frac{Ke^{-jk_0r_2}}{r_2} - K^2\frac{e^{-jk_0r_3}}{r_3}\right) \tag{10}$$

where (10) is a part (but not term by term) of the infinite series in (8b). The contribution from the remaining part of the infinite series will be included in the complex images discussed later.

C. Extraction of Surface Waves

R_{TE} and R_q in the integrands of (7) have poles on the real axis of the complex k_ρ plane. Extracting all the poles from R_{TE} and R_q, we can rewrite (7) as follows:

$$G_A^{xx} = G_{A0}^{xx} + G_{A,sw}^{xx} + \frac{\mu_0}{4\pi}\int_{-\infty}^{+\infty}\frac{1}{j2k_{z0}}F_1(k_\rho)e^{-jk_{z0}(z+z')} \cdot H_0^{(2)}(k_\rho\rho)k_\rho\,dk_\rho \tag{11a}$$

$$G_q = G_{q0} + G_{q,sw} + \frac{1}{4\pi\epsilon_0}\int_{-\infty}^{+\infty}\frac{1}{j2k_{z0}}F_2(k_\rho)e^{-jk_{z0}(z+z')} \cdot H_0^{(2)}(k_\rho\rho)k_\rho\,dk_\rho \tag{11b}$$

where

$$G_{A,sw}^{xx} = \frac{\mu_0}{4\pi}(-2\pi j)\,\mathrm{Res}_1\,H_0^{(2)}(k_{\rho p}\rho)k_{\rho p} \tag{12a}$$

$$G_{q,sw} = \frac{1}{4\pi\epsilon_0}(-2\pi j)\,\mathrm{Res}_2\,H_0^{(2)}(k_{\rho p}\rho)k_{\rho p} \tag{12b}$$

are the extracted terms corresponding to surface waves. Also, $k_{\rho p}$ is the surface wave pole located on the real axis of the complex k_ρ plane, and Res is the residue of the integrand in (7), at the pole $k_\rho = k_{\rho p}$. $F_1(k_\rho)$ and $F_2(k_\rho)$ are spectral-domain quantities with the quasi-dynamic part and surface waves extracted. In addition,

$$\mathrm{Res}_1 = \sum_{p(\mathrm{TE})}\left[\frac{e^{-jk_{z0}(z+z')}}{j2k_{z0}}\right]_{k_\rho = k_{\rho p}} \lim_{k_\rho \to k_{\rho p}}(k_\rho - k_{\rho p})R_{\mathrm{TE}} \tag{13a}$$

$$\mathrm{Res}_2 = \sum_{p(\mathrm{TE,TM})}\left[\frac{e^{-jk_{z0}(z+z')}}{j2k_{z0}}\right]_{k_\rho = k_{\rho p}} \cdot \lim_{k_\rho \to k_{\rho p}}(k_\rho - k_{\rho p})(R_{\mathrm{TE}} + R_q) \tag{13b}$$

$$F_1(k_\rho) = R_{\mathrm{TE}} - R_{\mathrm{TE}0} - \frac{2k_{\rho p}\,\mathrm{Res}_1}{k_\rho^2 - k_{\rho p}^2}j2k_{z0}e^{jk_{z0}(z+z')} \tag{14a}$$

$$F_2(k_\rho) = R_{\mathrm{TE}} + R_q - R_{\mathrm{TE}0} - R_{q0} - \frac{2k_{\rho p}\,\mathrm{Res}_2}{k_\rho^2 - k_{\rho p}^2}j2k_{z0}e^{jk_{z0}(z+z')}. \tag{14b}$$

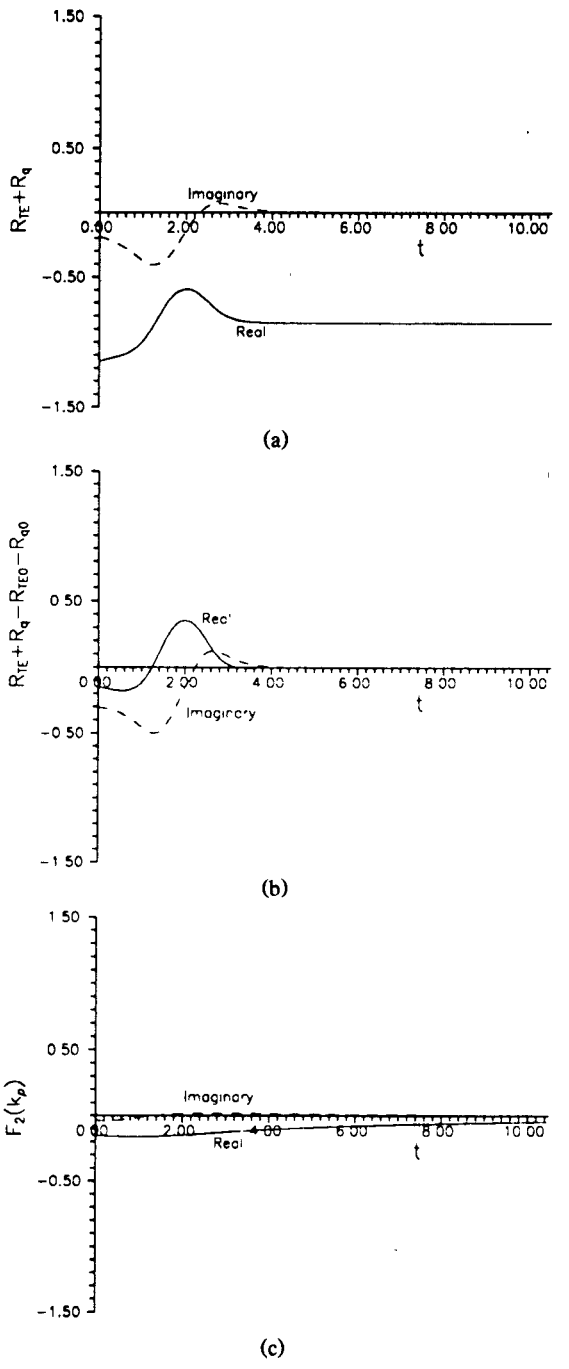

Fig. 3. (a) The behavior of the spectral function $(R_{\mathrm{TE}} + R_q)$ along the path C_1. (b) The spectral function $(R_{\mathrm{TE}} + R_q)$ with the quasi-dynamic term extracted. (c) The spectral function $(R_{\mathrm{TE}} + R_q)$ with the quasi-dynamic and surface wave terms extracted (see eq. (14b)).

The surface wave expressions have been used by Mosig and Gardiol [2] as a far-field approximation on the substrate interface. Here we take it as a constitutive part of the wave solution for all distances ρ.

D. Complex Images

The remaining integrals in (11) can be simulated by several complex images, similar to those in [5]. Here, in Fig. 2(a) and Fig. 2(b), we choose a finite path C_1 to be a straight line on the complex k_{z0} plane, which corresponds to a finite curve C_1 on the complex k_ρ plane. The parametric equation of the straight

TABLE I
AMPLITUDES a_i AND LOCATIONS b_i OF THREE COMPLEX IMAGES
($\epsilon_r = 12.6$, $h = 1$ mm, $f = 30$ GHz, $T_0 = 15.0$)

	G_A^{xx}				G_q			
	a_i		b_i		a_i'		b_i'	
i	Real Part	Imaginary Part	Real Part	Imaginary Part	Real Part	Imaginary Part	Real Part	Imaginary Part
1	−0.2760	−0.0022	−0.0453	0.0001	−0.0678	0.0068	−0.0523	0.0101
2	−0.6067	0.0100	−0.2624	−0.0015	−0.1548	−0.0151	−0.2712	−0.0139
3	0.8868	0.0547	−1.2064	−0.0897	0.0897	0.0171	−1.0598	−0.3165

line is

$$C_1: k_{z0} = k_0\left[-jt + \left(1 - \frac{t}{T_0}\right)\right], \qquad 0 \leq t \leq T_0 \tag{15}$$

where t is the running parameter and T_0 is the truncation point. T_0 should be larger than $\sqrt{\epsilon_r}$ to avoid the remnants of the extracted surface wave poles. Beyond this point, the choice of T_0 is quite arbitrary. In the numerical computation of this paper, T_0 is taken as 15. Other values of T_0 (eg., $T_0 = 5$ and 10) have been tried, and they give the same results for G_A^{xx} and G_q.

We now represent $F_1(k_\rho)$ and $F_2(k_\rho)$ by exponential forms of the complex variable k_{z0} of (15):

$$F_1(k_\rho) = \sum_{i=1}^{N} a_i e^{-b_i k_{z0}} = \sum_{i=1}^{N} A_i e^{B_i t} \tag{16a}$$

$$F_2(k_\rho) = \sum_{i=1}^{N} a_i' e^{-b_i' k_{z0}} = \sum_{i=1}^{N} A_i' e^{B_i' t} \tag{16b}$$

where

$$a_i = A_i e^{B_i T_0/1 + jT_0} \qquad b_i = B_i \frac{T_0}{k_0(1 + jT_0)} \tag{17}$$

and similarly for a_i' and b_i'. A complex function of a real variable of a finite range can be approximated by the summation of exponential functions, using Prony's method [9]. Therefore when the transformation of (15) changes the complex variable k_{z0} into a real variable t, Prony's method can be used.

Substituting (16) into (11) and using the Sommerfeld identity (to avoid the necessity of numerical integrations in k_ρ), we have

$$G_A^{xx} = G_{A0}^{xx} + G_{A,ci}^{xx} + G_{A,sw}^{xx} \tag{18a}$$

$$G_q = G_{q0} + G_{q,ci} + G_{q,sw} \tag{18b}$$

where

$$G_{A,ci}^{xx} = \frac{\mu_0}{4\pi} \sum_{i=1}^{N} a_i \frac{e^{-jk_0 r_i}}{r_i} \tag{19a}$$

$$G_{q,ci} = \frac{1}{4\pi\epsilon_0} \sum_{i=1}^{N} a_i' \frac{e^{-jk_0 r_i'}}{r_i'} \tag{19b}$$

$$r_i = \sqrt{\rho^2 + (z + z' - jb_i)^2} \qquad r_i' = \sqrt{\rho^2 + (z + z' - jb_i')^2}.$$

The subscript ci means complex image; r_i and r_i' are complex distances; and a_i and a_i' are complex amplitudes. Each term in (19) represents a complex image.

Expression (18) is the final closed-form spatial Green's function. it can be seen from (18) that G_A^{xx} or G_q is composed of three parts. The first part is the quasi-dynamic images, which are dominant in the near field region. The third part comprises the surface waves, which are dominant in the far field region of the substrate surface. The second part is very important in the intermediate region, and is related to leaky waves.

E. Discussion of the Behavior of $R_{TE} + R_q$

It is interesting to see the behavior of spectral function $R_{TE} + R_q$ along the path C_1 on the complex k_{z0} plane, since this spectral function embodies all the field characteristics on the microstrip substrate. Fig. 3(a) shows the behavior of $R_{TE} + R_q$ for a microstrip substrate ($\epsilon_r = 12.6$, $h = 1$ mm) at 30 GHz. Two salient features are observed. The first is that $R_{TE} + R_q$ does not vanish when k_ρ is large, which implies that the quasi-dynamic terms are involved. The second is that $R_{TE} + R_q$ has two sharp extrema along path C_1, which implies that the surface wave terms are involved. Fig. 3(b) shows the behavior of the spectral function ($R_{TE} + R_q - R_{TE0} - R_{q0}$) along path C_1, i.e., with the quasi-dynamic terms extracted. It can be seen that this function decays rapidly but still has the two sharp extrema. With the surface wave poles also extracted, Fig. 3(c) shows the behavior of the resulting function $F_2(k_\rho)$ along path C_1. It can be seen that the sharp extrema completely vanish, but the decay along C_1 is actually slower than that in Fig. 3(b). This spectral function $F_2(k_\rho)$ is associated with leaky waves. Despite the slow decay, we can simulate these leaky waves by a few complex images. Similar behavior is observed in $F_1(k_\rho)$.

III. NUMERICAL RESULTS

A microstrip substrate with $\epsilon_r = 12.6$, $h = 1$ mm is examined at three different frequencies ($f = 10$ GHz, 30 GHz, 50 GHz). A typical set of three complex images at 30 GHz with T_0 of (15) taken as 15 is listed in Table I.

Parts (a) and (b) of Fig. 4 show the amplitudes of the Green's functions computed by the closed forms (18) and by numerical integration. It can be seen that the difference between the closed-form Green's function and numerical integration is nearly unobservable; i.e., the difference is generally less than 1%. Many examples to check the precision of the closed-form Green's function (18) have been calculated. They are not included here because of limits on space.

IV. CONCLUSION

Through the Sommerfeld equality, plus some analytical and numerical techniques, a closed-form Green's function for thick microstrip substrate is presented. With this closed form, the numerical integration of the Sommerfeld integrals can be avoided completely, resulting in a significant reduction of computer time. A typical example is that, for the substrate of $\epsilon_r = 12.6$, $h/\lambda_0 = 0.1$, the closed-form Green's function for the scalar potential is only a ten-term expression: five terms for the

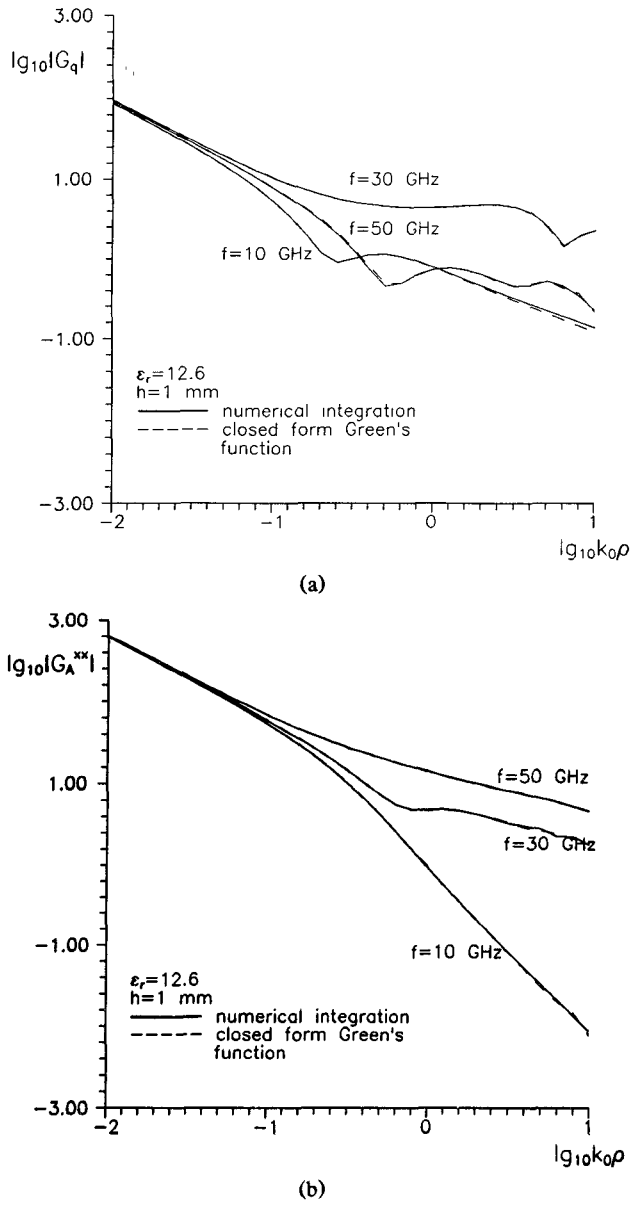

Fig. 4. (a) The amplitude of the scalar potential G_q. (b) The amplitude of the vector potential G_A^{xx}.

quasi-dynamic images (i.e., eq. (10)), three terms for the complex images (i.e., Table I), and two terms for the surface waves. The savings in computer time can be more than tenfold, with the error less than 1% compared with the numerical integration of the Sommerfeld integrals.

Finally, it should be pointed out that the closed-form equation (18) applies to all source-to-field distances on the substrate surface. As discussed in the Introduction, it is in the form $A + B + C$, representing the contributions of the quasi-dynamic images, the complex images, and the surface wave. At different distances, certain contributions may be small and can be dropped without causing much error in the spatial Green's function.

Acknowledgment

The authors thank the reviewers for many constructive comments.

References

[1] Y. L. Chow, "An approximate dynamic spatial Green's function in three dimensions for finite length microstrip lines," *IEEE Trans. Microwave Theory Tech.*, vol. MTT-28, pp. 393–397, 1980.
[2] J. R. Mosig and F. E. Gardiol, "A dynamical radiation model for microstrip structures," in *Advances in Electronics and Electron Physics*, vol. 59. London: Academic Press, 1982, pp. 139–239.
[3] P. B. Katehi and N. G. Alexopolous, "Real axis integration of Sommerfeld integrals with application to printed circuit antennas," *J. Math. Phys.*, vol. 24, pp. 527–533, 1983.
[4] E. Alanen and I. V. Lindell, "Exact image method for field calculation in horizontally layered medium above a conducting ground plane," *Proc. Inst. Elec. Eng.*, vol. 133, pt.H, pp. 297–304, 1986.
[5] D. G. Fang, J. J. Yang, and G. Y. Delisle, "Discrete image theory for horizontal electric dipoles in a multilayered medium," *Proc. Inst. Elec. Eng.*, vol. 135, pt. H, pp. 297–303, 1988.
[6] J. A. Stratton, *Electromagnetic Theory*. New York: McGraw-Hill, 1941, p. 576, eq. (17).
[7] J. Dai and Y. L. Chow, "A reduced model of a series of image charges for study MMIC's," in *Proc. Second Asia-Pacific Microwave Conf.* (Beijing, China), Oct. 26–28, 1988.
[8] J. Duncan, *The Elements of Complex Analysis*. New York: Wiley, 1968.
[9] R. W. Hamming, *Numerical Methods for Scientists and Engineers*. New York: Dover, 1973, pp. 620–622.

Measurement of Dielectric Constant Using a Microstrip Ring Resonator

P. A. Bernard and J. M. Gautray

Abstract —**A new approach for measuring the permittivity of dielectric materials by means of a microstrip ring resonator is presented. The method is used in conjunction with the variational calculation of the line capacitance of a multilayer microstriplike transmission line to compute the effective permittivity and hence the resonant frequency of the ring. The results are compared with measurements made in *X*-band waveguide cavity by cavity perturbation techniques.**

I. Introduction

Microstrip ring resonators are frequently employed in microwave integrated circuit design. Resonant structures such as rectangular, circular, and ring resonators have been widely studied in oscillators and filters [1]–[4]. The resonator is a large ring that is several wavelengths long to avoid mutual inductance effects [5] and problems caused by end effects in rectangular microstrip resonators. What is more, these ring resonators have Q factors of about 250, compared with 100 for rectangular ones.

The method presented here is based on the fact that the effective permittivity will change if the alumina/air boundary is modified by placing a dielectric material above the alumina substrate, thereby changing the resonant frequency of the ring. The variational calculation of the line capacitance [6], [7] is used to compute the effective permittivity of the multilayer microstriplike ring resonator and hence the resonant frequency for several test materials.

It is well known that the dielectric constant varies with frequency. Since we are very concerned with this frequency dependence, the test material above the Al_2O_3 substrate must be

Manuscript received February 5, 1990; revised July 9, 1990.
The authors are with the Universite de Bordeaux I, U.E.R. De Physique, Laboratoire De Physique Experimentale et Des Micro-Ondes, 351, Cours de la Liberation, 33405 Talence Cedex, France.
IEEE Log Number 9041947.